PHYSICAL REVIEW B VOLUME 47, NUMBER 5 1 FEBRUARY 1993-I

Comparison of Monte Carlo and diagrammatic calculations for the two-dimensional Hubbard model

N. Bulut
Institute for Theoretical Physics, University of California, Santa Barbara, California 93106

D. J. Scalapino
Department of Physics, University of California, Santa Barbara, California 93106

S. R. White
Department of Physics, University of California, Irvine, California 92717

(Received 10 July 1992)

Monte Carlo results for a two-dimensional Hubbard model in the intermediate-coupling regime $U=4t$ are compared with a diagrammatic spin-fluctuation approximation. Simulations on an 8×8 lattice doped away from half filling were carried out down to temperatures of order $\frac{1}{40}$ of the bandwidth. Results for the spin susceptibility $\chi(\mathbf{q},i\omega_m)$, the electron self-energy $\Sigma(\mathbf{p},i\omega_n)$, various pair-field susceptibilities, and the irreducible particle-particle scattering vertex $\Gamma(\mathbf{p}',i\omega_{n'}|\mathbf{p},i\omega_n)$ were obtained. A random-phase approximation for $\chi(\mathbf{q},i\omega_m)$ with a renormalized Coulomb coupling $\bar{U}$ is shown to provide a fit to the Monte Carlo data. A similar approximation for the Berk-Schrieffer spin-fluctuation interaction also provides a reasonable fit to the self-energy $\Sigma(\mathbf{p},i\omega_n)$ in the region explored by the Monte Carlo data. However, a similar approximation for the irreducible particle-particle interaction failed to reproduce the Monte Carlo results. Higher-order vertex corrections were calculated, but significant discrepancies with Monte Carlo results for Γ remain.

I. INTRODUCTION

The nature of the one-electron excitations and their effective interaction in a two-dimensional Hubbard model doped away from half filling remain open questions.[1] In the doped case, the fermion determinantal sign problem has made it difficult to carry out definitive numerical simulations.[2] However, various simulations have found evidence for short-range spin correlations, metallic behavior,[3] and short-range $d_{x^2-y^2}$ pair-field correlations.[4,5] Here we continue this study and compare Monte Carlo data for the spin susceptibility $\chi(\mathbf{q},i\omega_m)$, the one-electron self-energy $\Sigma(\mathbf{p},i\omega_n)$, various pair-field susceptibilities P_α, and the particle-particle scattering vertex $\Gamma(\mathbf{p}',i\omega_{n'}|\mathbf{p},i\omega_n)$ with diagrammatic approximations. We are particularly interested in determining to what extent a spin-fluctuation exchange approximation can reproduce the Monte Carlo results for these quantities in the intermediate-coupling regime. We will find that a random-phase-approximation (RPA) spin-fluctuation form for $\chi(\mathbf{q},i\omega_m)$ with a renormalized interaction $\bar{U}$ gives a good fit to the Monte Carlo data at intermediate coupling and at the temperatures that can be reached.[6] In addition, the corresponding Berk-Schrieffer[7] spin-fluctuation exchange interaction provides a reasonable fit to the one-electron self-energy. However, this renormalized single spin-fluctuation exchange interaction is significantly weaker than the measured particle-particle vertex $\Gamma(\mathbf{p}',i\omega_{n'}|\mathbf{p},i\omega_n)$ and underestimates the enhancement of the $d_{x^2-y^2}$-wave pair-field susceptibility P_d. In addition, we find that the leading vertex and crossed spin-fluctuation exchange contributions fail to provide a satisfactory fit of the Monte Carlo data for Γ.

To put these results in perspective, it is important to keep in mind the limitations on the momentum and energy resolution imposed by the finite size and temperature of the lattices on which the simulations have been carried out. The typical spatial lattice used in the Monte Carlo simulations is an 8×8 lattice. Physically, if each site is thought of as a Cu site, then this corresponds to roughly a 30 Å$\times$30 Å region. Alternatively, the $\Delta\mathbf{p}$ resolutions are $\frac{1}{8}$ of a reciprocal lattice vector. At half filling, $\langle n\rangle=\langle n_{i\uparrow}+n_{i\downarrow}\rangle=1$, where there is no fermion determinantal sign problem, one can easily go to temperatures $T=0.1$ in units of the hopping t. This corresponds to an energy scale of $\frac{1}{80}$ of the bandwidth. However, when the system is doped away from half filling (e.g., $\langle n\rangle=0.85$), the sign problem limits the temperature that can be reached. Typically the simulations we will discuss have $T=0.2$ corresponding to an energy of $\frac{1}{40}$ of the bandwidth.

In the intermediate-coupling regime, the two-dimensional Hubbard model has a high-energy scale set by the bandwidth $8t$ and an on-site Coulomb interaction U which is of order the bandwidth. Correspondingly, the short-distance scale is the lattice spacing. The next lower-energy scale is set by the exchange interaction energy $J\sim 4t^2/U$. For $U=4t$, this strong-coupling expression for J, while only approximate, gives $J\sim 1$ in units of t. Here and in the following we will measure energy in units of t. Thus a temperature $T\simeq 0.2$ is a factor of order 5 below J. However, depending upon the doping, the spin-fluctuation energy scale can be as much as an order of magnitude below J. Likewise the spin-fluctuation

correlation length can be of order the Monte Carlo lattice size. Thus calculations on 8×8 lattices with $T=0.2t$ are in a region where we should be able to begin to see the manifestations of the characteristic spin-fluctuation many-body effects. However, it will not be possible to reach definitive conclusions regarding the existence of Fermi-liquid behavior or superconducting pairing.

In Sec. II, we begin by examining the momentum, Matsubara frequency, and temperature dependence of the spin susceptibility $\chi(\mathbf{q},i\omega_m)$. We show that the Monte Carlo data can be fit using an RPA form with a reduced effective $\bar{U}$. In terms of this same effective $\bar{U}$, one can construct the Berk-Schrieffer[7] spin-fluctuation interaction. We then discuss the extent to which this interaction, neglecting vertex corrections, can describe the Monte Carlo results for the electron self-energy, various pair-field susceptibilities, and the effective particle-particle interaction. In Sec. III the nature of the short-range correlations produced by the particle-particle scattering and the effective value of $\bar{U}$ used in Sec. II are discussed. We find that it is important to include self-energy effects along with particle-particle scattering. Following this, the leading vertex corrections are calculated. Section IV contains our conclusions.

II. MONTE CARLO AND WEAK-COUPLING RESULTS

A. Magnetic susceptibility

At half filling, the ground state of the two-dimensional Hubbard model has long-range antiferromagnetic order.[8,9] When the system is doped away from half filling, Monte Carlo calculations show evidence for short-range, incommensurate antiferromagnetic fluctuations. These fluctuations can mediate an effective interaction between electrons. Thus we begin by examining the frequency- and wave-vector-dependent magnetic spin susceptibility

$$\chi(\mathbf{q},i\omega_m)=\int_0^\beta d\tau e^{i\omega_m\tau}\frac{1}{N}\sum_l e^{-i\mathbf{q}\cdot\mathbf{l}}\langle m_{i+l}^-(\tau)m_i^+(0)\rangle \ , \tag{1}$$

which characterizes the spin fluctuations. Here $m_i^+=c_{i\uparrow}^\dagger c_{i\downarrow}$, $m_i^+(\tau)=\exp(H\tau)m_i^+\exp(-H\tau)$, and $\omega_m=2m\pi T$ is the usual Matsubara Bose frequency.

Monte Carlo results for $\chi(\mathbf{q},0)$ with $U=4t$, $T=0.2t$ and an average site occupation of $\langle n\rangle\simeq0.87$ are shown in Fig. 1(a) for an 8×8 lattice. The inset shows the path in $\mathbf{q}$-space for which $\chi(\mathbf{q},0)$ is plotted. For this temperature and finite lattice size, the peak in $\chi(\mathbf{q},0)$ occurs at (π,π). However, the tendency towards an incommensurate structure in which the (π,π) peak splits and moves down the (q_x,π) and (π,q_y) edges rather than the $q_x=q_y$ diagonal is seen in the asymmetry of the curve. At this temperature, the results obtained for the 8×8 lattice are in close agreement with those on larger lattices except for $\mathbf{q}=(\pi,\pi)$, where the 8×8 result is of order 10% below the extrapolated bulk limit. Here we will concentrate on the 8×8 lattice, for which we have obtained a number of results.

A modified RPA form for χ, in which an effective Coulomb interaction $\bar{U}$ replaces U, provides a useful parametrization of the numerical Monte Carlo data.[10,6] Here

$$\chi_{\mathrm{RPA}}(\mathbf{q},i\omega_m)=\frac{\chi_0(\mathbf{q},i\omega_m)}{1-\bar{U}\chi_0(\mathbf{q},i\omega_m)} \ , \tag{2}$$

with $\chi_0(\mathbf{q},i\omega_m)$ the tight-binding Lindhard susceptibility

$$\chi_0(\mathbf{q},i\omega_m)=\frac{1}{N}\sum_p\frac{f(\varepsilon_{\mathbf{p}+\mathbf{q}})-f(\varepsilon_{\mathbf{p}})}{i\omega_m-(\varepsilon_{\mathbf{p}+\mathbf{q}}-\varepsilon_{\mathbf{p}})} \ . \tag{3}$$

For a square lattice with only a near-neighbor hopping t,

$$\varepsilon_{\mathbf{p}}=-2t(\cos p_x+\cos p_y) \ . \tag{4}$$

The Fermi factor $f(\varepsilon_{\mathbf{p}})=\{\exp[\beta(\varepsilon_{\mathbf{p}}-\mu)]+1\}^{-1}$, and μ is the chemical potential. The solid line in Fig. 1(a) shows $\chi_{\mathrm{RPA}}(\mathbf{q},0)$ calculated from Eqs. (2) and (3) for a filling of $\langle n\rangle=0.87$ on an infinite lattice at $T=0.2t$ with $\bar{U}=2t$. It is reasonable to expect that the effective Coulomb interaction is reduced by multiple particle-particle scattering, but what we find interesting is how well this approach also fits the $\mathbf{q}$, $i\omega_m$, and T dependence of $\chi(\mathbf{q},i\omega_m)$. Figure 1(b) shows Monte Carlo $\chi(\mathbf{q},i\omega_m)$ and $\chi_{\mathrm{RPA}}(\mathbf{q},i\omega_m)$ results for $\mathbf{q}=(\pi,\pi)$ versus ω_m. The decay of $\chi(\mathbf{q},i\omega_m)$ versus ω_m corresponds to a characteristic spin fluctuation frequency of order T, and the enhancement of $\chi(\mathbf{q}=(\pi,\pi),0)$ at $T=0.2t$ over the noninteracting result is approximately 5. Similar good agreement for the frequency dependence of $\chi(\mathbf{q},i\omega_m)$ is found for other values of $\mathbf{q}$. Figures 1(c) and 1(d) show $\chi(\mathbf{q},0)$ versus T for $\mathbf{q}=(\pi,\pi)$ and $\mathbf{q}=(0,0)$, respectively. Within RPA, $\chi(\mathbf{q},0)$ for $\mathbf{q}=(0,0)$ increases as T is lowered because of the presence of the Van Hove singularity at an energy $|\mu|$ above the noninteracting Fermi surface. For a filling of $\langle n\rangle=0.87$, $\mu\simeq-0.30t$. At a temperature that is roughly $|\mu|/4$, this growth in $\chi(\mathbf{q}=(0,0),0)$ stops. In Fig. 1(e), the finite-size dependence of the Monte Carlo data is shown for $T=0.25t$.

B. Single-particle self-energy

Monte Carlo simulations also give results for the single-particle thermal Green's function

$$G_{ij}(\tau)=-\langle Tc_{is}(\tau)c_{js}^\dagger(0)\rangle \ . \tag{5}$$

Here $c_{js}^\dagger$ creates an electron on the site j with spin s. Fourier transforming $G_{ij}(\tau)$ in both space and imaginary time gives

$$G(\mathbf{p},i\omega_n)=\frac{1}{i\omega_n-(\varepsilon_{\mathbf{p}}-\mu)-\Sigma(\mathbf{p},i\omega_n)} \ , \tag{6}$$

with $\omega_n=(2n+1)\pi T$. It is convenient to separate Σ into its real and imaginary parts,

$$\Sigma(\mathbf{p},i\omega_n)=[1-Z(\mathbf{p},i\omega_n)]i\omega_n-X(\mathbf{p},i\omega_n) \ . \tag{7}$$

The solid points in Fig. 2(a) is the wave-function renormalization parameter $Z(\mathbf{p},i\omega_n)$ versus ω_n for $\mathbf{p}=(3\pi/4,0)$. Figure 2(b) shows $X(\mathbf{p},i\omega_n)+\mu$. One can

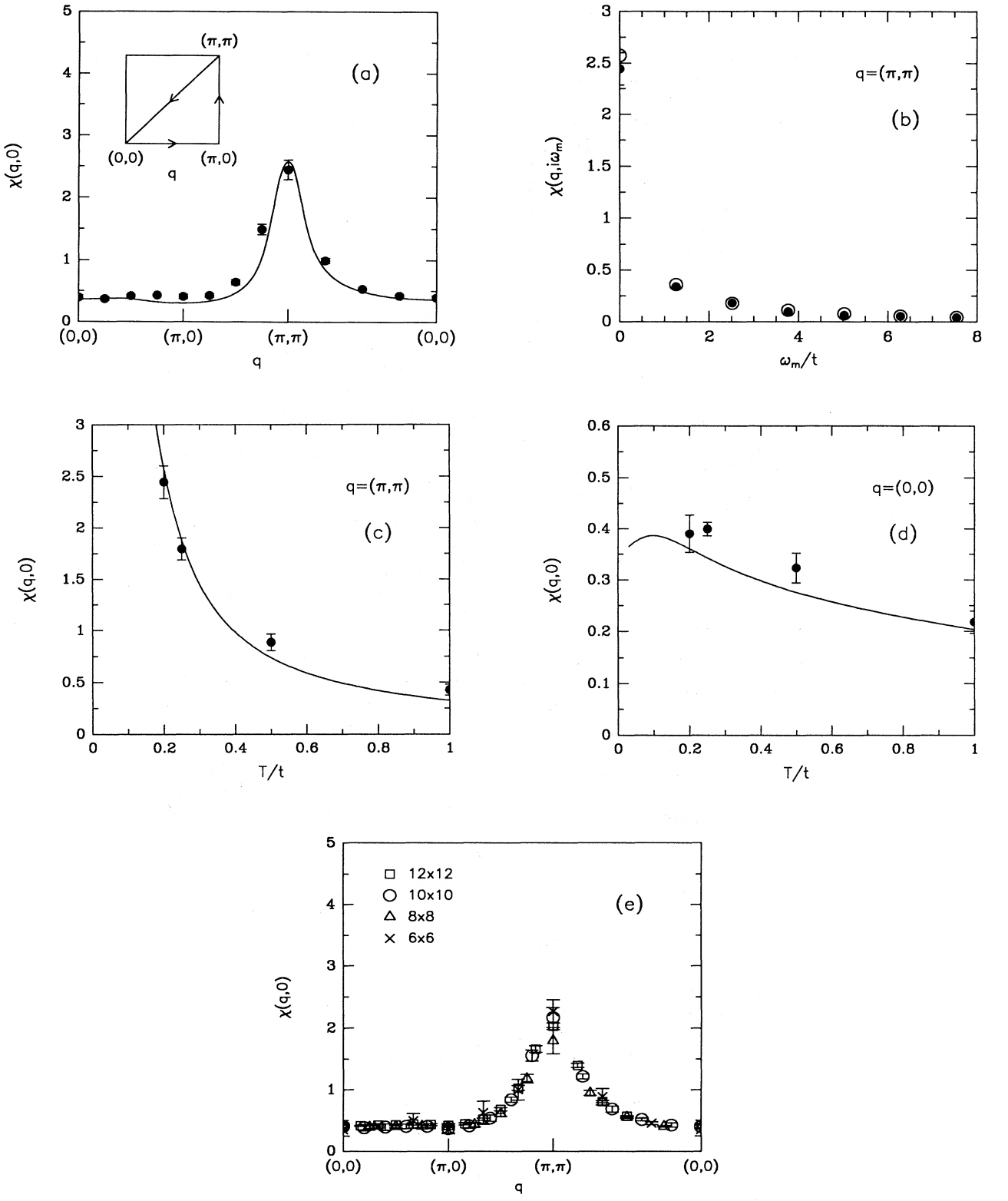

FIG. 1. (a) $\chi(\mathbf{q},0)$ vs $\mathbf{q}$ at $T=0.2t$ for the path in $\mathbf{q}$-space shown in the inset. (b) $\chi(\mathbf{q},i\omega_m)$ with $\mathbf{q}=(\pi,\pi)$ vs ω_m at $T=0.2t$. (c) $\chi(\mathbf{q},0)$ with $\mathbf{q}=(\pi,\pi)$ vs T. (d) $\chi(\mathbf{q},0)$ with $\mathbf{q}=(0,0)$ vs T. The solid points represent the Monte Carlo results obtained for $U=4t$ and $\langle n\rangle\simeq 0.87$ on an 8×8 lattice. The solid lines and the open circles represent the RPA results obtained for $\bar{U}=2t$ and $\langle n\rangle=0.87$ on an infinite lattice. (e) Finite-size dependence of the Monte Carlo data for $\chi(\mathbf{q},0)$ at $T=0.25t$.

think of $X(\mathbf{p},i\omega_n)+\mu$ as the effective chemical potential of the interacting system. As seen in Fig. 2(b), at high frequencies it decays to a constant.

As expected, $Z(\mathbf{p},i\omega_n)$ approaches 1 at Matsubara frequencies which are large compared to the spin-fluctuation frequency. At low frequency, $Z(\mathbf{p},i\omega_n)$ increases and contributes to the mass enhancement of the quasiparticles. At present we do not have Monte Carlo data on sufficiently large lattices[11] at low temperatures to determine the low-temperature scaling behavior of $Z(\mathbf{p},i\omega_n)$. If it remains finite on the Fermi surface, then one has a Fermi liquid.

The leading spin-fluctuation contributions to the self-energy are shown in Fig. 3. The first, Hartree, term simply shifts the chemical potential, while the remaining terms in the top and bottom row of graphs correspond to the Berk-Schrieffer[7] longitudinal and transverse spin-fluctuation contributions, respectively. Including the

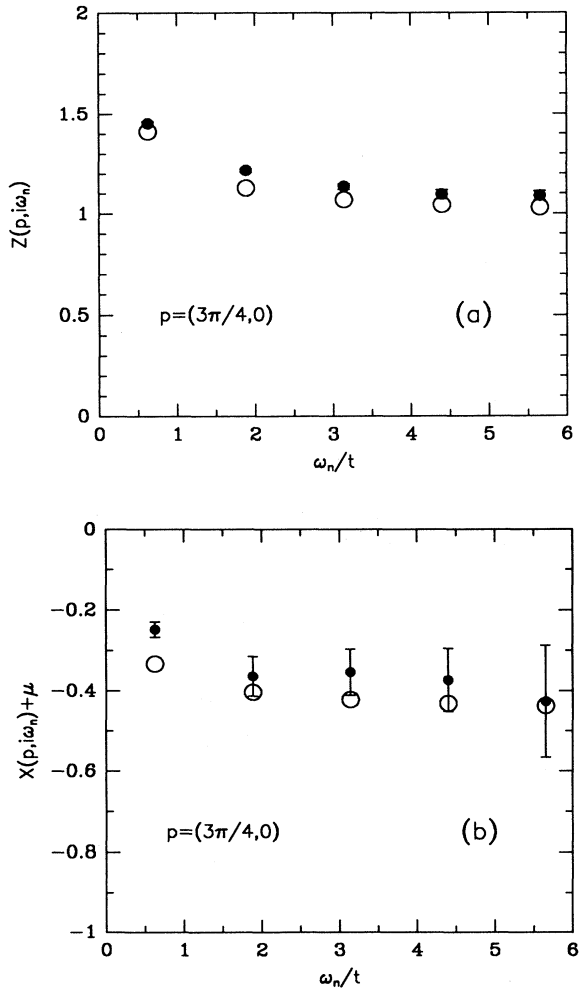

FIG. 2. (a) Wave-function renormalization parameter $Z(\mathbf{p},i\omega_n)$ and (b) $X(\mathbf{p},i\omega_n)+\mu$ vs ω_n for $\mathbf{p}=(3\pi/4,0)$ on an 8×8 lattice at $\langle n\rangle\simeq0.87$. Here the solid points are the Monte Carlo data and the open circles are the results obtained from Eq. (8) with $U=4t$ replaced by $\bar{U}=2t$ in Eq. (9).

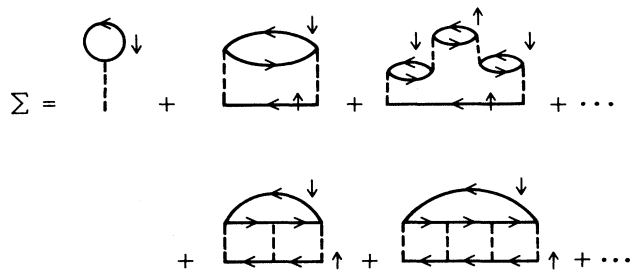

FIG. 3. Contributions to the self-energy $\Sigma(p)$ given by Eq. (8).

Hartree term in μ, the contribution to Σ from the diagrams shown in Fig. 3 is

$$\Sigma(\mathbf{p},i\omega_n)=\frac{T}{N}\sum_{\mathbf{q},m}V(\mathbf{q},i\omega_m)G_0(\mathbf{p}-\mathbf{q},i\omega_n-i\omega_m)\ , \tag{8}$$

with $G_0^{-1}(\mathbf{p},i\omega_n)=i\omega_n-(\varepsilon_{\mathbf{p}}-\mu)$ and

$$V(\mathbf{q},i\omega_m)=\frac{U^2\chi_0(\mathbf{q},i\omega_m)}{1-U^2\chi_0^2(\mathbf{q},i\omega_m)}+\frac{U^3\chi_0^2(\mathbf{q},i\omega_m)}{1-U\chi_0(\mathbf{q},i\omega_m)}\ . \tag{9}$$

Just as in the RPA treatment of χ, multiple particle-particle scattering reduces U. Here we will replace U in Eq. (9) by the effective $\bar{U}$ determined from fitting the Monte Carlo results for χ.

Using G_0 in Eq. (8) neglects the rainbow contributions and the vertex corrections to Σ. One could argue that the spin-fluctuation energy is small compared to the Fermi energy. However here, contrary to Migdal's well-known approximation[12] for the electron-phonon problem, nesting and Van Hove singularities can give rise to a significant momentum dependence of Σ and may lead to enhanced vertex corrections. Thus this procedure is an uncontrolled approximation. However, in Sec. III B we will study the contribution of the lowest-order spin-fluctuation vertex corrections to the self-energy and see that it is of order 10% in this regime of the Hubbard model. Results for $Z(\mathbf{p},i\omega_n)$ and $X(\mathbf{p},i\omega_n)=\mu$ on an 8×8 lattice obtained without taking into account the vertex corrections are compared with the Monte Carlo data in Fig. 2.

C. Particle-particle correlations

The Berk-Schrieffer single-spin fluctuation exchange contributions to the irreducible particle-particle interaction Γ_I are shown in Fig. 4 and are given by

$$\Gamma_I(p'|p)=U+\frac{U^3\chi_0^2(p'-p)}{1-U^2\chi_0^2(p'-p)}+\frac{U^2\chi_0(p'+p)}{1-U\chi_0(p'+p)}\ . \tag{10}$$

Here we are using a notation in which $p=(\mathbf{p},i\omega_n)$. As before, we will replace U by $\bar{U}$ in the second and third terms. The first term remains the bare U since $\bar{U}$ is not two-particle irreducible, and iterating on U in the two-particle channel will reproduce the terms associated with $\bar{U}$.

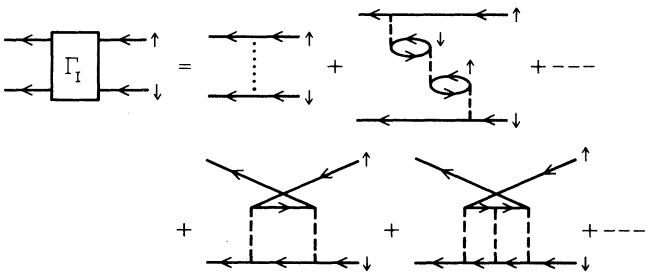

FIG. 4. Single spin-fluctuation exchange interaction. The dotted line represents the bare Coulomb repulsion U, and the dashed lines are the reduced Coulomb repulsion $\bar{U}$.

The approximate Γ_I, Eq. (10), can be compared with the Monte Carlo data in an indirect way by using it to compute the pair-field susceptibilities

$$P_\alpha = \int_0^\infty d\tau \langle \Delta\alpha(\tau)\Delta_\alpha^\dagger(0)\rangle \ , \tag{11}$$

with

$$\Delta_\alpha^\dagger = \sum_{\mathbf{p}} g_\alpha(\mathbf{p}) c_{\mathbf{p}\uparrow}^\dagger c_{-\mathbf{p}\downarrow}^\dagger \ . \tag{12}$$

Here we use for a local s wave $g_s(\mathbf{p})=1$ and for a $d_{x^2-y^2}$ wave $g_d(\mathbf{p})=(\cos p_x - \cos p_y)/2$. We have calculated P_α by summing the diagrams shown in Fig. 5. The double line in Fig. 5 is the single-particle Green's function dressed with the spin-fluctuation self-energy and the box is Γ_I. We have also calculated $\bar{P}_\alpha$, shown in Fig. 5, which contains only the dressed single-particle propagators. Both P_α and $\bar{P}_\alpha$ can be obtained from the Monte Carlo simulations,[5] and results comparing P_α and $\bar{P}_\alpha$ are shown in Fig. 6.

As seen in Fig. 6(a), the Coulomb repulsion strongly suppresses the s-wave pair-field susceptibility. The enhancement of the $d_{x^2-y^2}$-wave pair-field susceptibility seen in Fig. 6(b) shows that the effective interaction between the quasiparticles in this channel is attractive. Here the weak-coupling calculation overestimates $\bar{P}$ and P. However, their difference $P-\bar{P}$ is a factor of 2 smaller than the Monte Carlo results. This suggests that the effective interaction is larger than the single spin-fluctuation exchange result.

A direct approach for obtaining Monte Carlo results for the irreducible particle-particle interaction involves calculating the two-particle Green's function

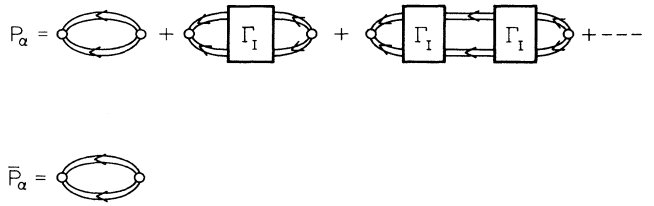

FIG. 5. Diagrammatic approximation for P_α. Here the double lines denote the single-particle Green's function dressed with Σ and the box is Γ_I of Fig. 4. Also illustrated is $\bar{P}_\alpha$ which does not include the particle-particle interaction vertices.

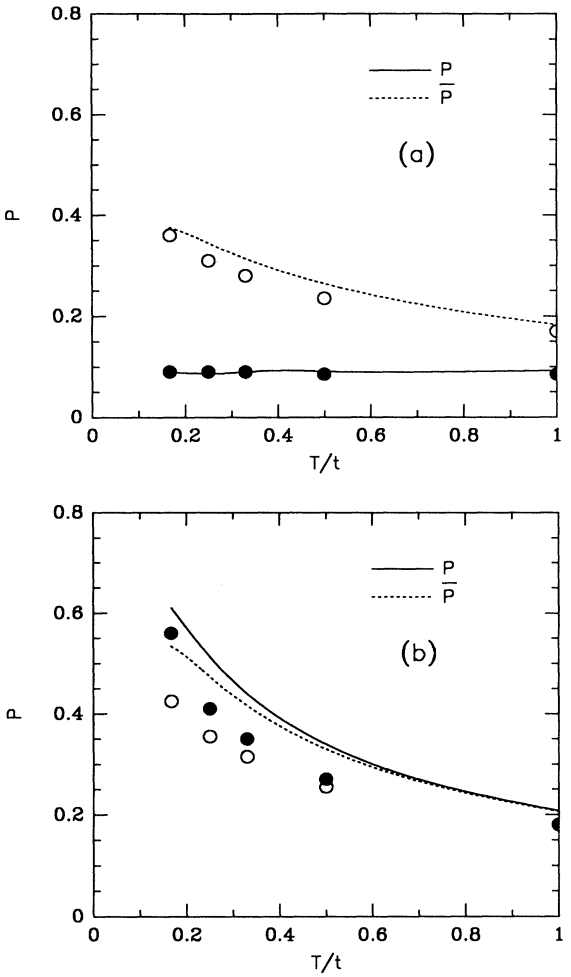

FIG. 6. P_α and $\bar{P}_\alpha$ vs T for (a) s and (b) $d_{x^2-y^2}$-wave form factors on an 8×8 lattice at $\langle n\rangle \simeq 0.87$. The solid and open points are the Monte Carlo data for P_α and $\bar{P}_\alpha$, respectively, obtained using $U=4t$. The solid and the dotted curves are the corresponding diagrammatic results for $U=4t$ and $\bar{U}=2t$.

$$\Lambda(3,4|1,2) = -\langle T c_{i_4\uparrow}(\tau_4) c_{i_3\downarrow}(\tau_3) c_{i_2\downarrow}^\dagger(\tau_2) c_{i_1\uparrow}^\dagger(\tau_1)\rangle \ . \tag{13}$$

Then, Fourier transforming on both the space and imaginary time variables allows us to determine

$$\begin{aligned}\Lambda(p',k'|p,k) = &-\delta_{p,p'}\delta_{k,k'} G_\uparrow(p) G_\downarrow(k) \\ &+ \frac{T}{N}\delta_{k',p+k-p'} G_\uparrow(p') G_\downarrow(k') \\ &\times \Gamma(p',k'|p,k) G_\uparrow(p) G_\downarrow(k) \ ,\end{aligned} \tag{14}$$

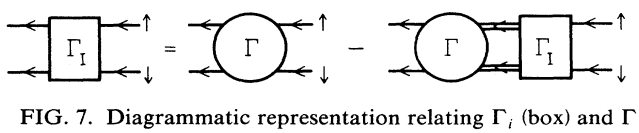

FIG. 7. Diagrammatic representation relating Γ_i (box) and Γ (circle). Here the double lines are dressed single-particle propagators. Usually one selects an approximate form for Γ_I and solves for Γ. However, the Monte Carlo calculation gives Γ and G so that we will solve this equation to obtain Γ_I.

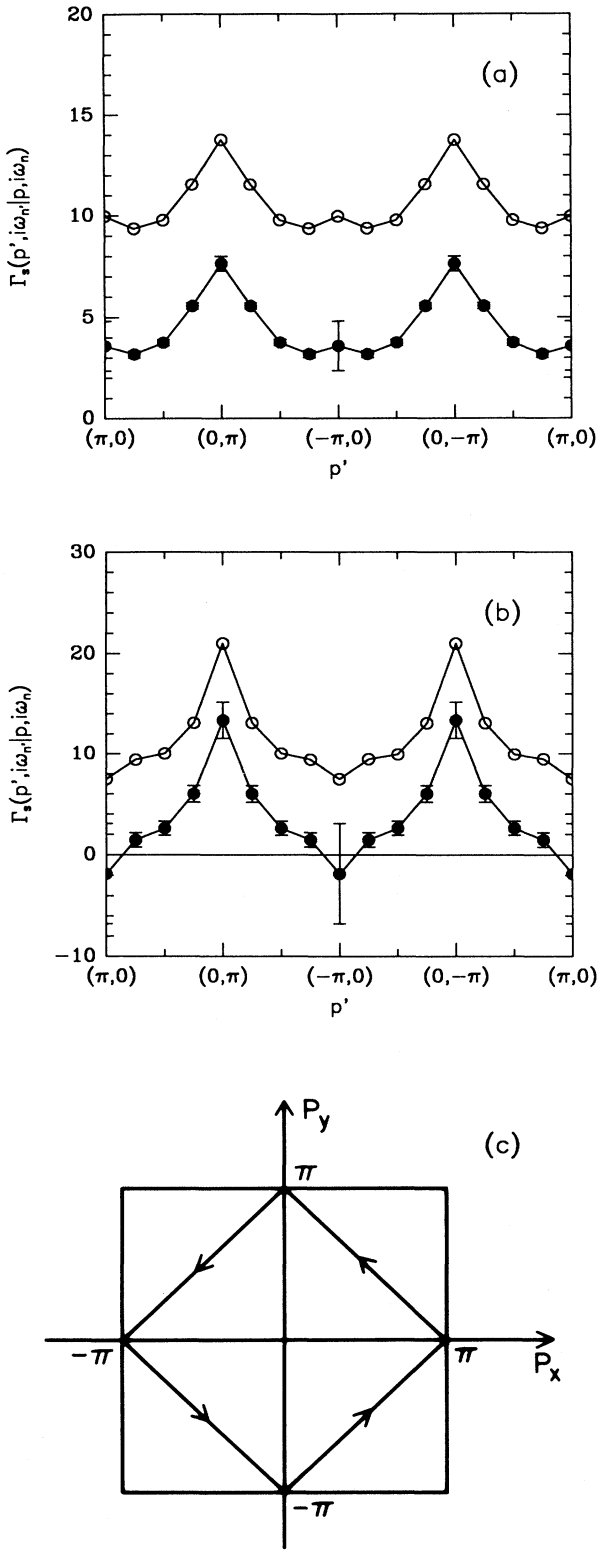

FIG. 8. Monte Carlo results for the reducible and the irreducible particle-particle interaction in the singlet channel, $\Gamma_s(p'|p)$ and $\Gamma_{I,s}(p'|p)$, on an 8×8 lattice with $U=4t$ and $\langle n\rangle\simeq0.87$ at (a) $T=0.50t$ and (b) $0.25t$. Here $p=(\mathbf{p},i\pi T)$ with $\mathbf{p}=(\pi,0)$ and $p'=(\mathbf{p}',i\pi T)$ with $\mathbf{p}'$ taken along the path shown in (c).

from which one can obtain the reducible particle-particle vertex $\Gamma(p',k'|p,k)$. Here $p=(\mathbf{p},i\omega_n)$ and we will calculate the particle-particle interaction in the zero center-of-mass momentum and energy channel, hence we set $k=-p$ and $k'=-p'$. In order to obtain the irreducible particle-particle vertex Γ_I, we use the Monte Carlo results for Γ and G to solve the diagrammatic equation shown in Fig. 7,

$$\Gamma_I(p'|p)=\Gamma(p'|p)+\frac{T}{N}\sum_k\Gamma(p'|k)G(k)G(-k)\Gamma_I(k|p)\,, \tag{15}$$

where $\Gamma(p'|p)$ is used as a short notation for $\Gamma(p',-p'|p,-p)$. This procedure is essentially the opposite one from the usual diagrammatic approach in which an irreducible vertex such as Γ_I is selected and then Γ is calculated from Eq. (15).

Using Monte Carlo results for $\Gamma(p'|p)$ and $G(\mathbf{p},i\omega_n)$

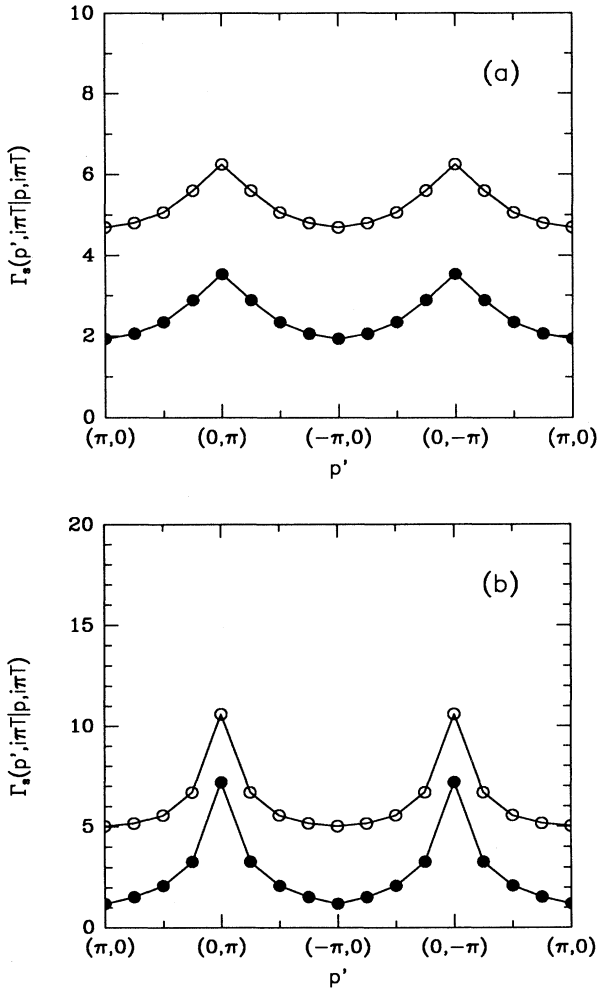

FIG. 9. Diagrammatic results for the reducible $\Gamma_s(p'|p)$ and the irreducible $\Gamma_{I,s}(p'|p)$ in the particle-particle channel assuming that the dominant interaction in the particle-particle channel is the single spin-fluctuation exchange. Here results are shown from an 8×8 lattice with $U=4t$, $\bar{U}=2t$, and $\langle n\rangle=0.87$ at (a) $T=0.50t$ and (b) $T=0.25t$.

we have solved the integral equation, Eq. (15), for Γ_I on an 8×8 lattice with $U=4t$ and $\langle n\rangle \simeq 0.87$. Symmetrizing Γ_I gives the irreducible interaction in the singlet channel

$$\Gamma_{Is}(p'|p)=\tfrac{1}{2}(\Gamma_I(p'|p)+\Gamma_I(-p'|p)) \ . \tag{16}$$

In Fig. 8(a), both the reducible $\Gamma_s(p'|p)$ and the irreducible $\Gamma_{Is}(p'|p)$ in the singlet channel are plotted as a function of $\mathbf{p}'$ for $\omega_n=\omega_{n'}=\pi T$ at $T=0.50t$. Results at $T=0.25t$ are shown in Fig. 8(b). In these plots p' follows the contour shown in Fig. 8(c), while $\mathbf{p}$ is kept fixed at $(\pi,0)$. The large error bars for $\mathbf{p}'=(\pi,0)$ and $(-\pi,0)$ arise from the need to subtract out the first term in Eq. (14) for these wave vectors. Similar results are shown in Figs. 9(a) and 9(b) for the single spin-fluctuation exchange interaction. One observes that the single spin fluctuation exchange result is about a factor of 2 smaller than the Monte Carlo data. While replacing $U=4$ by $\bar{U}=2$ in the susceptibility provided a sensible fit to the Monte Carlo data, it is clear that this simple procedure fails to reproduce the effective particle-particle interaction.

III. HIGHER-ORDER CORRECTIONS

The diagrammatic calculations described in Sec. II are based upon using a renormalized Coulomb interaction $\bar{U}$ which is chosen to fit the RPA form for $\chi(\mathbf{q},i\omega_m)$ to the Monte Carlo results. Physically, the reduced $\bar{U}$ takes into account the Coulomb correlations, which act to suppress double occupation of a site. Kanamori[13] suggested that this renormalization can be approximated by replacing U by the particle-particle t matrix. Here we will examine this for the Hubbard model and show that in addition to the t matrix, self-energy effects and vertex corrections are required. We will then calculate the lowest-order vertex corrections and examine their effects on Σ and the irreducible singlet particle-particle pairing interaction.

A. Magnetic susceptibility within Kanamori's approach

For an interacting system $\chi(\mathbf{q},i\omega_m)$ can be written as

$$\chi(\mathbf{q},i\omega_m)=-\frac{T}{N}\sum_p G(p+q)G(p) + \left[\frac{T}{N}\right]^2 \sum_{p,p'} G(p'+q)G(p')\bar{\Gamma}_q(p'|p) \times G(p+q)G(p) \ . \tag{17}$$

Here $\bar{\Gamma}_q(p'|p)$ is the reducible particle-hole t matrix with a center-of-mass momentum and energy $q=(\mathbf{q},i\omega_m)$, and $G(p)$ is the single-particle Green's function. The reducible $\bar{\Gamma}_q(p'|p)$ in turn can be expressed in terms of the irreducible particle-hole vertex $\bar{\Gamma}_{I,q}(p'|p)$:

$$\bar{\Gamma}_q(p'|p)=\bar{\Gamma}_{I,q}(p'|p) - \frac{T}{N}\sum_k \bar{\Gamma}_{I,q}(p'|k)G(k+q)G(k)\bar{\Gamma}_q(k|p) \ . \tag{18}$$

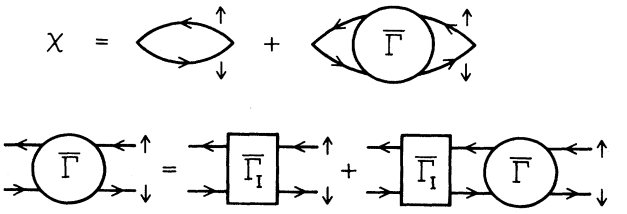

FIG. 10. Feynmann diagrams contributing to $\chi(\mathbf{q},i\omega_m)$ and the t-matrix equation expressing the reducible $\bar{\Gamma}$ in terms of the irreducible $\bar{\Gamma}_I$ in the particle-hole channel.

Feynmann diagrams representing Eqs. (17) and (18) are given in Fig. 10. The random-phase approximation amounts to assuming that $\bar{\Gamma}_{I,q}(p'|p)$ is a constant and equal to the bare interaction strength U. Kanamori[13] showed, within the context of ferromagnetic fluctuations in an itinerant model, that the renormalization of the strong Coulomb repulsion at the cost of kinetic energy can be diagrammatically taken into account by summing the set of particle-particle t-matrix diagrams shown in Fig. 11. The contribution of these diagrams to $\bar{\Gamma}_I$ can be expressed by

$$\bar{\Gamma}_{I,q}(p'|p)=\frac{U}{1+UP(\mathbf{q},i\omega_m)} \ , \tag{19}$$

which is independent of p' and p and only depends on q. Here $P(\mathbf{q},i\omega_m)$ is given by

$$P(\mathbf{q},i\omega_m)=\frac{T}{N}\sum_p G(p+q)G(-p) \ . \tag{20}$$

Ordinarily, one would use Eq. (19) for $\bar{\Gamma}_I$ to calculate $\bar{\Gamma}$ and then use it to obtain $\chi(\mathbf{q},i\omega_m)$. Because of the $\mathbf{q}$ dependence of $\bar{\Gamma}_I$, a closed form analytic expression for $\chi(\mathbf{q},i\omega_m)$ is not obtainable. However, Chen *et al.*[6] suggested that an approximate solution for $\chi(\mathbf{q},i\omega_m)$ is the RPA expression of Eq. (2) with $U_{\rm red}$, given by

$$U_{\rm red}\equiv\frac{U}{1+U\langle P_0(\mathbf{q},0)\rangle_{\mathbf{q}}} \ . \tag{21}$$

substituted for $\bar{U}$. Here, P_0 is obtained from Eq. (20) using the noninteracting Green's function $G_0(p)$, and the average of $P_0(\mathbf{q},0)$ is taken over the whole Brillouin zone. The reduced Coulomb interaction $U_{\rm red}$ calculated in this fashion, is dependent on the filling and the temperature. Figure 12 shows the temperature dependence of $U_{\rm red}$ for $\langle n\rangle=0.87$ and $U=4t$ on an infinite lattice. We observe that at low temperatures, and especially around $T\sim 0.2t$, the value of $U_{\rm red}(T)$ is very close to $2t$. Hence the fit to Monte Carlo data on $\chi(\mathbf{q},i\omega_m)$ that we have seen in Sec. II is consistent with this approximation.

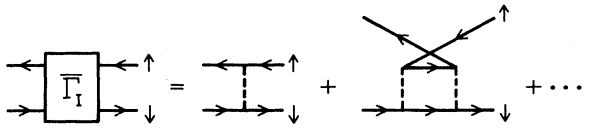

FIG. 11. Multiple particle-particle scatterings contributing to the particle-hole irreducible Γ_I in Kanamori's approach.

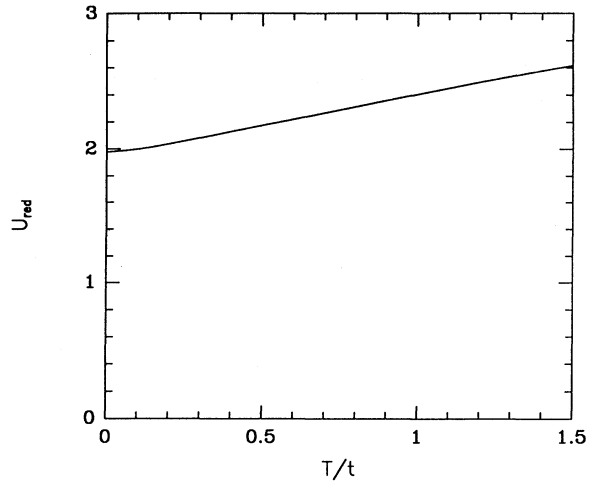

FIG. 12. Temperature dependence of $U_{\rm red}(T)$ as given by Eq. (22) for $U=4t$, $\langle n \rangle = 0.87$ on an infinite lattice.

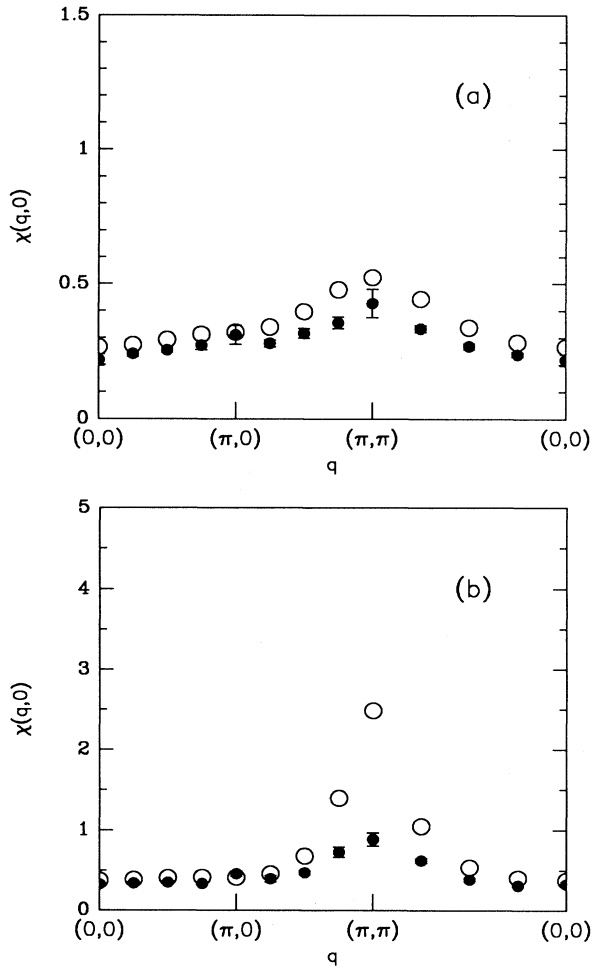

FIG. 13. Momentum dependence of $\chi(\mathbf{q},0)$ obtained from the numerical solution of Eqs. (18)–(20) using the bare Green's function $G_0(\mathbf{p},i\omega_n)$ (open circles) compared to Monte Carlo data (full circles). Here results are given on an 8×8 lattice for $U=4t$, $\langle n \rangle \simeq 0.87$, (a) $T=1t$ and (b) $T=0.50t$.

It is possible to numerically solve Eqs. (17) and (18) for $\chi(\mathbf{q},i\omega_m)$ on an 8×8 lattice using $\bar{\Gamma}_I$ of Eq. (19). Results for $\chi(\mathbf{q},0)$ vs $\mathbf{q}$ obtained using the bare Green's function

$$G_0(p)=\frac{1}{i\omega_n-(\varepsilon_{\rm p}-\mu)} \tag{22}$$

in Eqs. (17) and (18) are given in Figs. 13(a)–13(b). We see that this more exact approach to calculating $\chi(\mathbf{q},0)$ does not give as good agreement with Monte Carlo as using the RPA form for $\chi(\mathbf{q},i\omega_m)$ with the expression $U_{\rm red}$ of Eq. (21). Next we solve Eqs. (17) and (18) using the Green's functions obtained from Monte Carlo simulations. These Green's functions have the full self-energy due to spin fluctuations. Using $G_{\rm MC}(p)$'s corresponds to basically dressing the G's with spin fluctuations. The results, in this case, are shown in Figs. 14(a)–14(b). The agreement with Monte Carlo results is significantly better than what we have seen in Figs. 13(a)–13(b) using the bare propagators.[14] Here $\chi(\mathbf{q},0)$ calculated perturbatively is smaller than the Monte Carlo data. This is in agreement with the notion that higher-order corrections to the

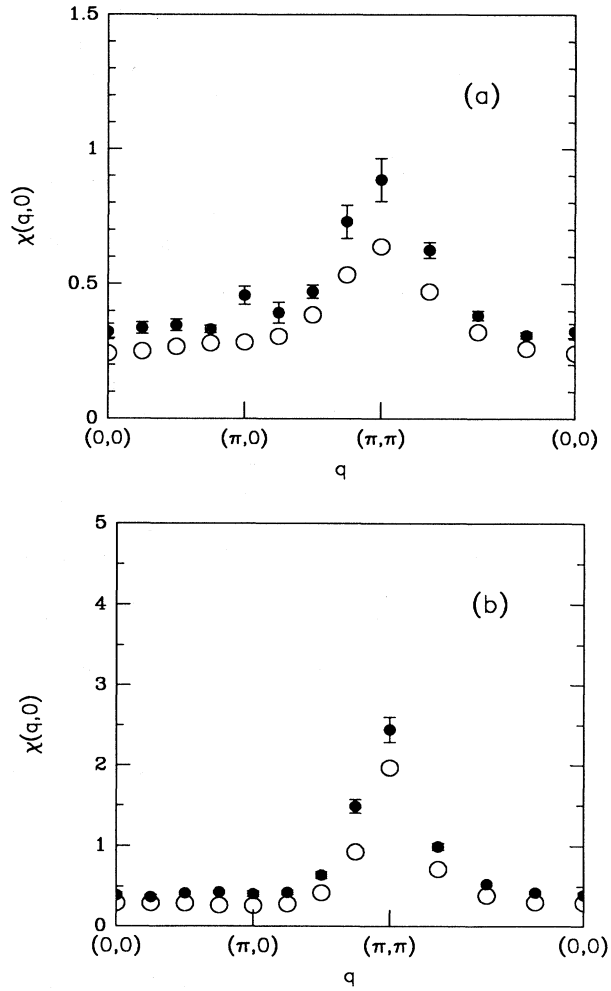

FIG. 14. Same as in Fig. 13 but using the Monte Carlo Green's function, which includes the exact self-energy due to the Coulomb repulsion, at (a) $T=0.50t$ and (b) $T=0.20t$.

interaction, which are left out in this calculation, enhance $\chi(\mathbf{q},0)$.

Thus while replacing U by $\bar{U}$ in a RPA form for χ provides a useful fit of the Monte Carlo data, piecemeal approximations such as the t-matrix approximation actually make things worse. One must keep t-matrix, self-energy, and vertex corrections on the same footing in order to achieve a reasonable fit. This suggests that conserving approximations are required.[15]

B. Higher-order contributions to the single-particle self-energy and the irreducible particle-particle vertex

In Sec. II B, we calculated the lowest-order spin-fluctuation contributions to the single-particle self-energy and the particle-particle interaction. Here we examine this approximation by computing the next-order diagrams in the spin-fluctuation exchange, and compare them with the lowest-order results. We find that these higher-order contributions to Σ are small in the parameter space of the Hubbard model that we are studying. In addition, we find that the second-order corrections are not sufficient to fit the Monte Carlo results for the particle-particle interaction. Yonemitsu[16] has carried out similar calculations but for different parameter values. He also finds that these corrections enhance the RPA behavior.

The second-order spin-fluctuation corrections to the self energy, labeled $\Sigma^{(2a)}(p)$ and $\Sigma^{(2b)}(p)$, are shown diagrammatically in Fig. 15. Here $\gamma^{(a)}(p'|p)$ and $\gamma^{(b)}(p'|p)$ are the vertex corrections illustrated in Fig. 16. Analytic expressions for these diagrams are given in the Appendix. Their overall contribution to the self-energy is $2\Sigma^{(2a)}(p)+\Sigma^{(2b)}(p)$. The resultant $Z(\mathbf{p},i\omega_n)$ and $X(\mathbf{p},i\omega_n)+\mu$ versus ω_n for $\mathbf{p}=(3\pi/4,0)$ are shown in Fig. 17. We see that while the corrections to these quantities are small, they improve the agreement with the Monte Carlo data.

To second order in the exchange of spin-fluctuations, there are contributions to Γ_I from vertex corrections and also from diagrams involving the crossed exchange of two spin fluctuations.[17] The leading vertex corrections $\Gamma_I^{(2a)}$ and $\Gamma_I^{(2b)}$ are given in Fig. 18. The diagrams involving the crossed exchange of spin fluctuations, $\Gamma^{(Xa)}$ and $\Gamma^{(Xb)}$ are shown in Fig. 19. These are of special interest, since they have been proposed to mediate the pairing in the

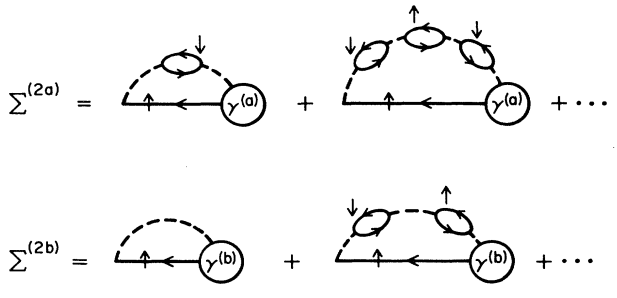

FIG. 15. Diagrammatic representation of the lowest-order vertex corrections to $\Sigma(\mathbf{p},i\omega_n)$.

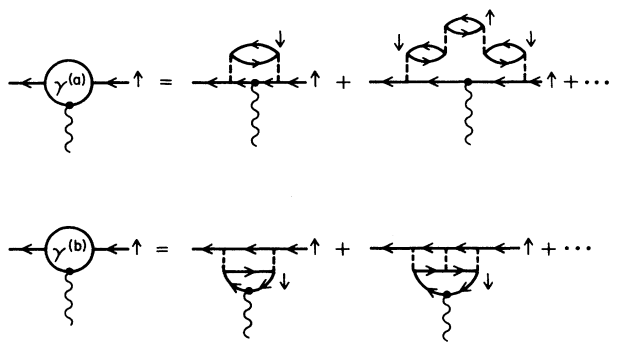

FIG. 16. Diagrammatic representation of $\gamma^{(a)}(p'|p)$ and $\gamma^{(b)}(p'|p)$.

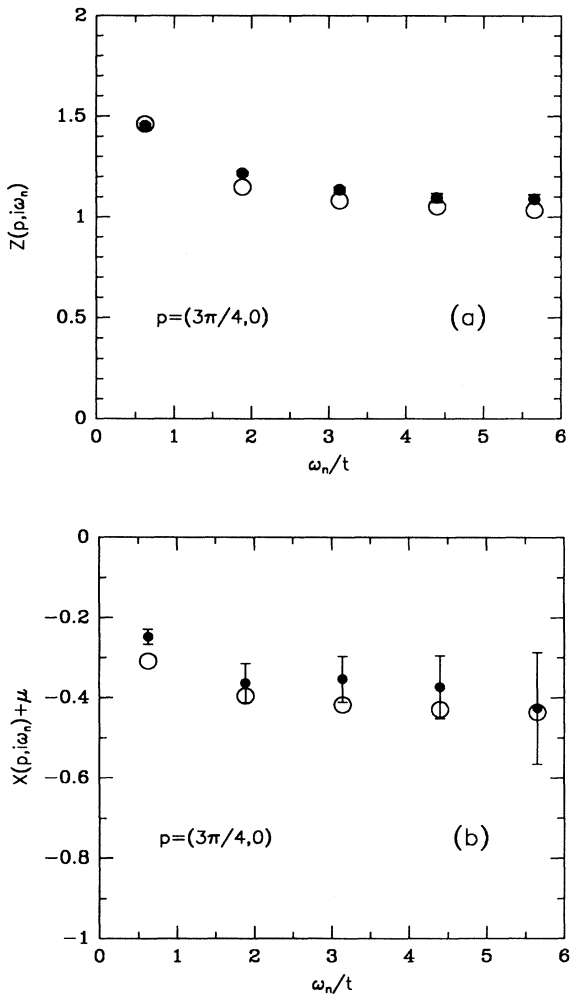

FIG. 17. (a) Wave-function renormalization parameter $Z(\mathbf{p},i\omega_n)$ and (b) $X(\mathbf{p},i\omega_n)+\mu$ vs ω_n/t for $\mathbf{p}=(3\pi/4,0)$ on an 8×8 lattice for $\bar{U}=2t$, $\langle n\rangle\simeq0.87$, and $T=0.2t$. Here $Z(\mathbf{p},i\omega_n)$ and $X(\mathbf{p},i\omega_n)+\mu$ have been calculated by including the effects of the vertex corrections.

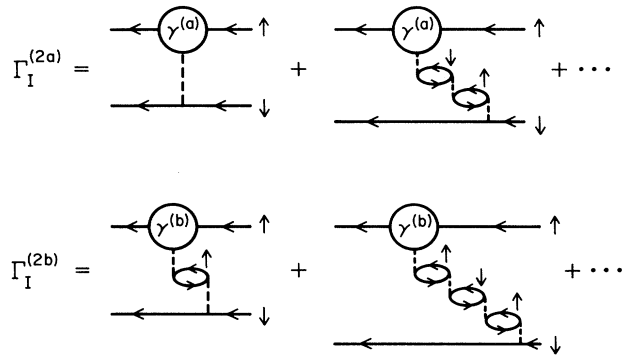

FIG. 18. Diagrammatic representation of the vertex corrections to the single spin-fluctuation exchange interaction.

spin bags picture[18,17] in the weak-coupling limit of the Hubbard model. The contributions to Γ_I from the vertex corrections and the crossed diagrams are $\Gamma_I^{(2)}=2\Gamma_I^{(2a)}+\Gamma_I^{(2b)}$ and $\Gamma_I^{(X)}=\Gamma_I^{(Xa)}+2\Gamma_I^{(Xb)}$, respectively.

In order to explore these corrections and their possible low-temperature behavior we have used a 128×128 lattice for $T=0.20t$ and $0.10t$. In Figs. 20(a)–20(c) we compare the magnitudes of the vertex corrections and the crossed diagrams with the single spin-fluctuation exchange interaction of Eq. (10) in the singlet channel for $\omega_n=\omega_{n'}=\pi T$. In these figures $\theta_{\mathbf{p}'}=\tan^{-1}(p_y'/p_x')$, and $\mathbf{p}$ is kept on the Fermi surface along the (1,0) direction. The single spin-fluctuation exchange interaction shown in Fig. 20(a) peaks for (π,π) momentum transfer and has a large constant background of order $5t$. The vertex-correction contributions shown in Fig. 20(b) is smaller in magnitude and peaks for momentum transfers $\mathbf{q}\sim(0,0)$. The contribution from the crossed diagrams, shown in Fig. 20(c), exhibits the momentum structure proposed by Kampf and Schrieffer;[17] it is repulsive for momentum transfers $\mathbf{q}\sim(\pi,\pi)$ and attractive for $\mathbf{q}\sim(0,0)$, both by direct scattering and via umklapp. However, its magnitude is small[19] relative to the lowest-order contributions shown in Fig. 20(a). Hence, even though the second-order corrections give better results for $\Sigma(p)$, the underlying particle $\Sigma(p)$, the underlying particle-particle interaction is still underestimated by the spin-fluctuation exchange interaction including second-order contributions.

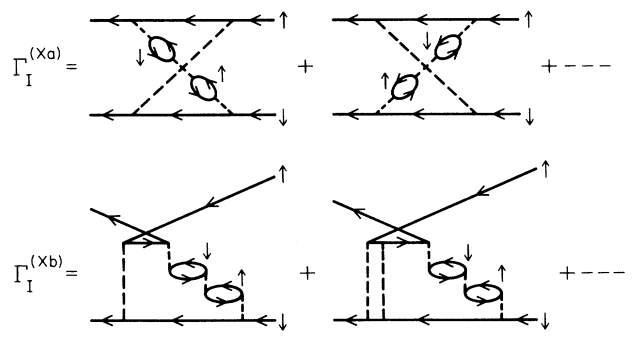

FIG. 19. Diagrammatic representation of the crossed exchange of two spin fluctuations.

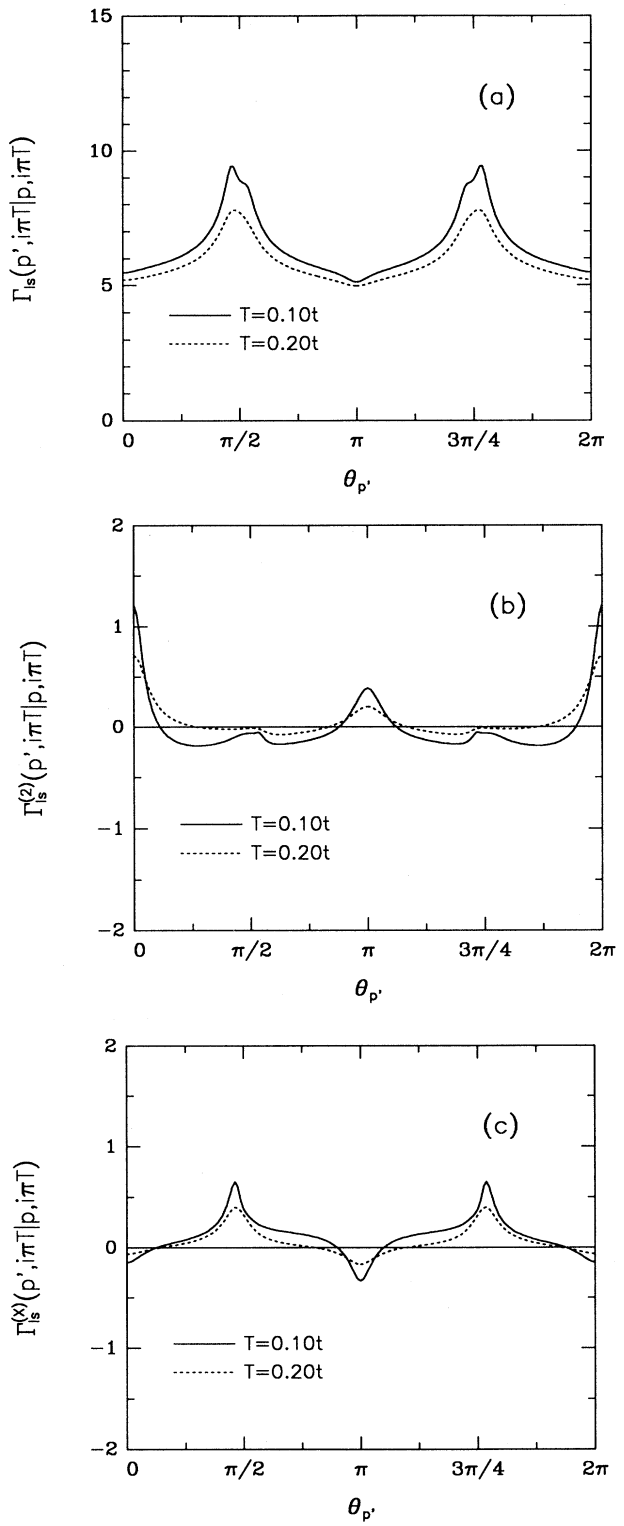

FIG. 20. (a) Momentum dependence of the irreducible particle-particle interaction in the singlet channel, $\Gamma_{I,s}(p'|p)$, for the single spin-fluctuation exchange. Here $p=(\mathbf{p},i\pi T)$ with $\mathbf{p}=(p_F,0)$ and $p'=(\mathbf{p}',i\pi T)$ with $\mathbf{p}'$ taken on the Fermi surface. Also $\theta_{\mathbf{p}'}=\tan^{-1}(p_y'/p_x')$, $U=4t$, $\bar{U}=2t$, $\langle n\rangle=0.87$, and $T=0.10t$ and $0.20t$. (b) Same as in (a) but for $\Gamma_{Is}^{(2)}(p'|p)$. (c) Same as in (a) but for $\Gamma_{Is}^{(X)}(p'|p)$.

IV. CONCLUSIONS

In this paper we have compared the results obtained from quantum Monte Carlo simulations for $\chi(\mathbf{q},i\omega_m)$, $\Sigma(\mathbf{p},i\omega_n)$, various pair-field susceptibilities, and the particle-particle scattering vertex $\Gamma(\mathbf{p}',i\omega_{n'}|\mathbf{p},i\omega_n)$ with diagrammatic spin-fluctuation calculations. In the intermediate-coupling regime $U=4t$, we found that the spin susceptibility $\chi(\mathbf{q},i\omega_m)$ could be fit by an RPA-like form with a reduced interaction $\bar{U}=2t$. Good agreement for the momentum, frequency, and temperature dependence was found for temperatures down to $T=0.2t$. In the remainder of the paper, we addressed the question of whether the same type of renormalized weak-coupling theory can also describe the single-particle and the particle-particle properties of the Hubbard model in the regime of interest. For this purpose we first calculated the single-particle self-energy to first order in the spin-fluctuation exchange. Reasonable agreement with the Monte Carlo results for the quasiparticle renormalization $Z(\mathbf{p},i\omega_n)$ and the effective chemical potential $X(\mathbf{p},i\omega_n)+\mu$ were obtained. An indirect comparison of the particle-particle interaction was obtained by comparing the s- and $d_{x^2-y^2}$-wave pair-field susceptibilities down to $T\sim 0.2t$. In this regime of the Hubbard model, pairing correlations in the singlet channel with $d_{x^2-y^2}$-wave orbital symmetry are enhanced by the on-site Coulomb repulsion, while the s-wave pair-field susceptibility is suppressed.

The relative enhancement of P_d over $\bar{P}_d$ obtained from the Monte Carlo calculations is larger than that predicted from the single spin-fluctuation exchange. In order to obtain further information on the nature of the particle-particle interactions, we have used Monte Carlo results to determine the irreducible particle-particle interaction vertex. Here we see a clear failure of the single spin-fluctuation exchange, which gives a significantly weaker scattering. However, this is not in contradiction with the agreement obtained for Σ, since it involves a different average of Γ_I. When one compares $P_d-\bar{P}_d$ or directly Γ_I, one sees that the spin-fluctuation exchange underestimates the effective particle-particle interaction. We have also seen that the second-order spin-fluctuation corrections are not sufficiently strong to make up for the difference between the Monte Carlo data and the lowest-order spin-fluctuation exchange.

APPENDIX

The second-order spin-fluctuation correction to Σ is $\Sigma^{(2a)}(p)+2\Sigma^{(2b)}(p)$, where

$$\Sigma^{(2a)}(p)=\frac{T}{N}\sum_k G_0(k)\frac{U^2\chi_0(k-p)}{1-U^2\chi_0^2(k-p)}\gamma^{(a)}(p|k)\ , \tag{A1}$$

and

$$\Sigma^{(2b)}(p)=-\frac{T}{N}\sum_k G_0(k)\frac{U}{1-U^2\chi_0^2(k-p)}\gamma^{(b)}(p|k) \tag{A2}$$

with

$$\gamma^{(a)}(p'|p)=\frac{T}{N}\sum_k G(k)G(k-p+p')\frac{U^2\chi_0(k-p)}{1-U^2\chi_0^2(k-p)} \tag{A3}$$

and

$$\gamma^{(b)}(p'|p)=\frac{T}{N}\sum_k G(k)G(k-p+p')\frac{U^2\chi_0(k-p)}{1-U\chi_0(k-p)}\ . \tag{A4}$$

Because of the minus sign in Eq. (A2), the contributions from $\Sigma^{(2a)}(p)$ and $\Sigma^{(2b)}(p)$ interfere to give a weaker effect.

Similarly, the second-order vertex correction to Γ_I is $\Gamma_I^{(2)}=2\Gamma_I^{(2a)}+\Gamma_I^{(2b)}$, where

$$\Gamma_I^{(2a)}(p'|p)=\frac{T}{N}\sum_k G(k)G(k+p'-p)\frac{U^2\chi_0(k-p)}{1-U^2\chi_0^2(k-p)}\times\left[\frac{U}{1-U^2\chi_0^2(p'-p)}+\frac{U^2\chi_0(k+p')}{1-U\chi_0(k+p')}\right] \tag{A5}$$

and

$$\Gamma_I^{(2b)}(p'|p)=\frac{T}{N}\sum_k G(k)G(k+p'-p)\frac{U^2\chi_0(k-p)}{1-U\chi_0(k-p)}\times\frac{U^2\chi_0(p'-p)}{1-U^2\chi_0^2(p'-p)}\ . \tag{A6}$$

Just as for $\Sigma^{(2a)}(p)$ and $\Sigma^{(2b)}(p)$, $\Gamma_I^{(2a)}$ and $\Gamma_I^{(2b)}$ have different signs. This reduces the effect of the total vertex correction on Γ_I.

Finally, the contributions from the crossed diagrams are $\Gamma_I^{(X)}=\Gamma_I^{(Xa)}+2\Gamma_I^{(Xb)}$, where

$$\Gamma_I^{(Xa)}(p'|p)=-\frac{T}{N}\sum_k G(k)G(k-p'-p)\frac{U}{1-U^2\chi_0^2(k-p)}\times\frac{U}{1-U^2\chi_0^2(k-p')}-U^2\chi_0(p'+p) \tag{A7}$$

and

$$\Gamma_I^{(Xb)}(p'|p)=-\frac{T}{N}\sum_k G(k)G(k-p'-p)\frac{U^2\chi_0(p'+p)}{1-U\chi_0(p'+p)}\times\frac{U}{1-U^2\chi_0^2(k-p')}-\frac{U^3\chi_0^2(p'+p)}{1-U\chi_0(p'+p)}\ . \tag{A8}$$

ACKNOWLEDGMENTS

We thank N. E. Bickers and J. R. Schrieffer for useful discussions. This work was partially supported by the National Science Foundation under Grants Nos. DMR90-02492 and PHY89-04035, and the Electrical Power Research Institute. N. B. gratefully acknowledges financial support from IBM. S. R.W. would like to thank the office of Naval Research for support under Grant No. N00014-91-J-1143. This research was also supported in part by the University of California through an allocation of computer time. The numerical calculations reported in this paper were primarily performed at the San Diego Supercomputer Center.

[1] *High Temperature Superconductivity,* edited by K. S. Bedell, D. Coffey, D. Meltzer, D. Pines, and J. R. Schrieffer (Addison-Wesley, Reading, MA, 1990); M^2 S-HTSC III Proceedings (North-Holland, Amsterdam, 1991).

[2] E. Y. Loh, J. E. Gubernatis, R. T. Scalettar, S. R. White, D. J. Scalapino, and R. L. Sugar, Phys. Rev. B **41**, 9301 (1990).

[3] D. J. Scalapino, in *High Temperature Superconductivity,* edited by K. S. Bedell, D. Coffey, D. E. Meltzer, D. Pines, and J. R. Schrieffer (Addison-Wesley, Reading, MA, 1990), p. 314.

[4] M. Imada and Y. Hatsugai, J. Phys. Soc. Jpn. **58**, 3752 (1989); N. Furukawa and M. Imada, Physica C **185-189**, 1443 (1991).

[5] S. R. White, D. J. Scalapino, R. L. Sugar, N. E. Bickers, and R. T. Scalettar, Phys. Rev. B **39**, 839 (1989).

[6] L. Chen, C. Bourbonnais, T. Li, and A.-M. S. Tremblay, Phys. Rev. Lett. **66**, 369 (1991).

[7] N. F. Berk and J. R. Schrieffer, Phys. Rev. Lett. **17**, 433 (1966).

[8] J. E. Hirsch and S. Tang, Phys. Rev. Lett. **62**, 591 (1989).

[9] S. R. White, D. J. Scalapino, R. L. Sugar, E. Y. Loh, J. E. Gubernatis, and R. T. Scaletar, Phys. Rev. B **40**, 506 (1989).

[10] N. Bulut, in *Dynamics of Magnetic Fluctuations in High Temperature Superconductors,* edited by G. Reiter, P. Horsch, and G. Psaltakis (Plenum, New York, 1991).

[11] Larger lattices are also required in order to determine the locus of Fermi surface wave vectors.

[12] A. B. Migdal, Zh. Eksp. Teor. Fiz. **34**, 1438 (1958) [Sov. Phys. JETP **7**, 996 (1958)].

[13] J. Kanamori, Prog. Theor. Phys. **30**, 275 (1963).

[14] B. S. Shastry, J. Phys. F **9**, 1367 (1979), has shown that in the Kanamori approximation for the magnetic susceptibility, using the bare single-particle Green's functions violates the Ward identities, while including the self-energy restores the Ward identities.

[15] N. E. Bickers and D. J. Scalapino, Ann. Phys. (N.Y.) **193**, 206 (1989).

[16] K. Yonemitsu, J. Phys. Soc. Jpn. **58**, 4576 (1989).

[17] A. Kampf and J. R. Schrieffer, Phys. Rev. B **41**, 6399 (1990).

[18] J. R. Schrieffer, X.-G. Wen, and S. C. Zhang, Phys. Rev. B **39**, 11 663 (1989).

[19] Similar small corrections were obtained for the 8×8 lattice at the temperatures for which Monte Carlo data are available.